Check for updates

AGU ADVANCING EARTH AND SPACE SCIENCE

Geophysical Research Letters

RESEARCH LETTER
10.1029/2020GL090947

A New Approach to Constrain the Seismic Origin for Prehistoric Turbidites as Applied to the Dead Sea Basin

Yin Lu[1,2], Jasper Moernaut[2], Revital Bookman[3], Nicolas Waldmann[3], Nadav Wetzler[4], Amotz Agnon[5], Shmuel Marco[6], G. Ian Alsop[7], Michael Strasser[2], and Aurélia Hubert-Ferrari[1]

[1]Department of Geography, University of Liege, Liège, Belgium, [2]Department of Geology, University of Innsbruck, Innsbruck, Austria, [3]Dr. Moses Strauss Department of Marine Geosciences, University of Haifa, Haifa, Israel, [4]Geological Survey of Israel, Jerusalem, Israel, [5]The Neev Center for Geoinfomatics, Institute of Earth Sciences, Hebrew University of Jerusalem, Jerusalem, Israel, [6]Department of Geophysics, Tel Aviv University, Tel Aviv, Israel, [7]Department of Geology & Geophysics, University of Aberdeen, Scotland, UK

Abstract The seismic origin of turbidites is verified either by correlating such layers to historic earthquakes, or by demonstrating their synchronous deposition in widely spaced, isolated depocenters. A historic correlation could thus constrain the seismic intensity required for triggering turbidites. However, historic calibration is not applicable to prehistoric turbidites. In addition, the synchronous deposition of turbidites is difficult to test if only one deep core is drilled in a depocenter. Here, we propose a new approach that involves analyzing the underlying *in situ* deformations of prehistoric turbidites, as recorded in a 457 m-long core from the Dead Sea center, to establish their seismic origin. These *in situ* deformations have been verified as seismites and could thus authenticate the trigger for each overlying turbidite. Moreover, our high-resolution chemical and sedimentological data validate a previous hypothesis that soft-sediment deformation in the Dead Sea formed at the sediment-water interface.

Plain Language Summary Seismogenic turbidites are widely used for geohazard assessment. The use of turbidites as an earthquake indicator requires a clear demonstration that an earthquake, rather than non-seismic factors, is the most plausible trigger. The seismic origin is normally verified either by correlating the turbidites to historic earthquakes, or by demonstrating their synchronous deposition in widely spaced, isolated depocenters. The correlated historic earthquakes could thus constrain the seismic intensities necessary for triggering turbidites. However, the historic correlation method is not applicable to prehistoric turbidites. In addition, the synchronous deposition of turbidites cannot be verified if only one deep core is drilled in a depocenter. Here, we propose a new approach to constrain the seismic origin for prehistoric turbidites in a deep core from the Dead Sea center. Moreover, we constrain the seismic intensities that triggered prehistoric turbidites by analyzing the degree of *in situ* deformation underlying each turbidite. In addition, we use our results to propose seven basic earthquake-related depositional scenarios preserved in depocenters located in tectonically active regions like the Dead Sea. These techniques and findings permit a more confident geohazard assessment in the region and other similar tectonic settings by improving the completeness of a paleoseismic archive.

Key Points:

- Seismic origin for prehistoric turbidites is established by analyzing the underlying *in situ* deformation structures for each turbidite
- Data validate a previous hypothesis that soft-sediment deformation formed at the sediment-water interface in the Dead Sea
- The new approach permits a more confident geohazard assessment by improving the completeness of a paleoseismic archive

Supporting Information:

- Supporting Information S1

Correspondence to:
Y. Lu,
yin.lu@uibk.ac.at;
yinlusedimentology@yeah.net

Citation:
Lu, Y., Moernaut, J., Bookman, R., Waldmann, N., Wetzler, N., Agnon, A. et al. (2021). A new approach to constrain the seismic origin for prehistoric turbidites as applied to the Dead Sea Basin. *Geophysical Research Letters*, *48*, e2020GL090947. https://doi.org/10.1029/2020GL090947

Received 22 SEP 2020
Accepted 23 NOV 2020

© 2020. The Authors.
This is an open access article under the terms of the Creative Commons Attribution License, which permits use, distribution and reproduction in any medium, provided the original work is properly cited.

1. Introduction

Seismogenic turbidites are commonly used to derive information such as location, timing, intensity and recurrence intervals of paleoearthquakes, and are thus vital for geohazard assessment (Goldfinger et al., 2003; St-Onge et al., 2004; Gràcia et al., 2010; Polonia et al., 2013; Strasser et al., 2013; Pouderoux et al., 2014; Ratzov et al., 2015; Moernaut et al., 2018; Hubert-Ferrari et al., 2020). However, the use of turbidites as an earthquake indicator requires a demonstration that seismicity is the most plausible trigger, rather than non-seismic factors such as flash floods (Talling et al., 2013; Katz et al., 2015), exceptional discharge (Clare et al., 2016), and storm waves (Paull et al., 2018). This challenge is generally overcome by correlating turbidites with historic earthquakes in a region (Gràcia et al., 2010; Moernaut et al., 2014; Polonia et al., 2016; Wilhelm et al., 2016) or by demonstrating their synchronous deposition in widely spaced, isolated depocenters (Goldfinger et al., 2007; Ratzov et al., 2015; Kioka et al., 2019).

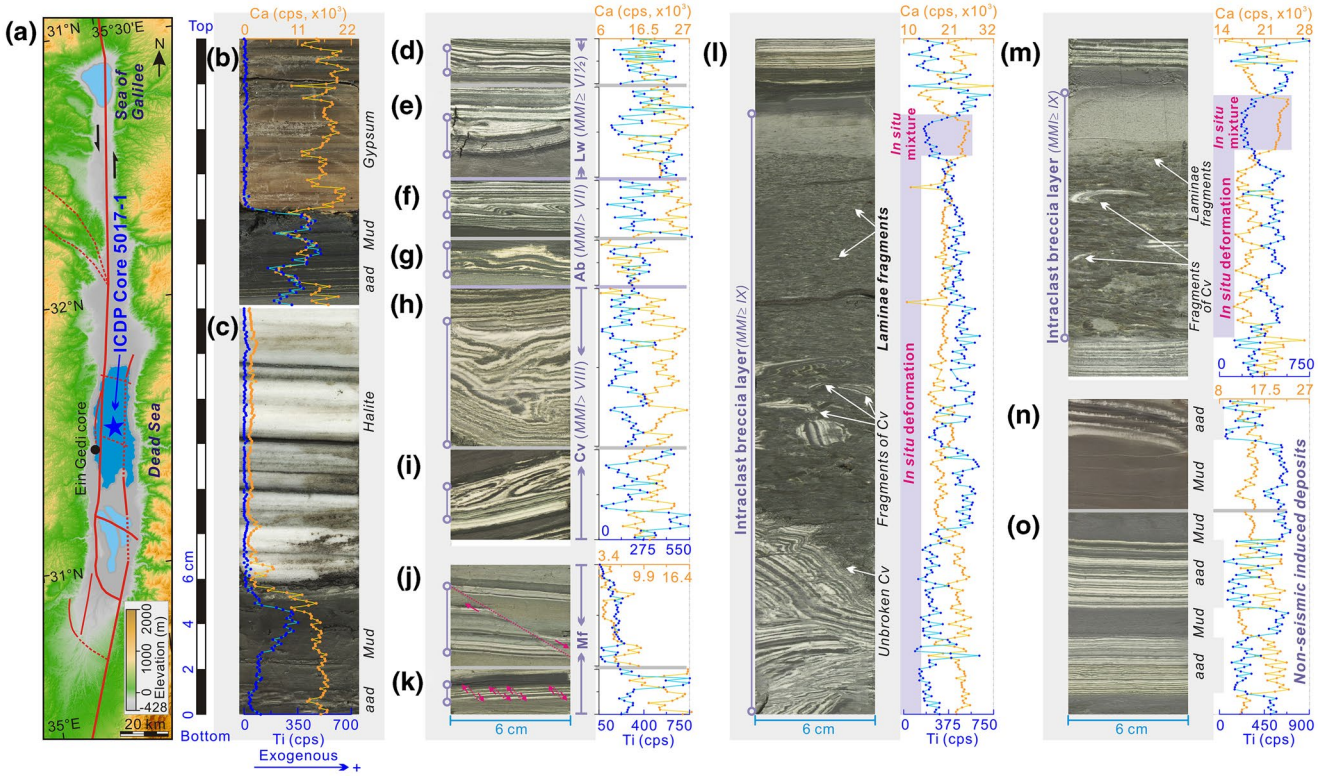

Figure 1. Tectonic setting of the Dead Sea Basin (a) and chemical data characterizing *in situ* seismites (d–m) (Lu et al., 2020b) and background deposits (b-c, n-o) in Core 5017-1. (a) Active faults in the basin (Bartov et al., 2006; Ben-Avraham et al., 2008). (b) Gypsum. (c) Halite. (d–m) *In situ* seismites: (d)–(e) linear waves (Lw); (f)–(g) asymmetric billows (Ab); (h)–(i) coherent vortices (Cv); (j)–(k) Micro-faults (Mf); (l–m) intraclast breccias (Ib). (n–o) Background deposits; *aad*, alternating laminae of aragonite and detritus; cps, count per second. See Text S3 for core depth.

The seismic intensities required for triggering turbidites are normally constrained by the correlated earthquakes (Moernaut et al., 2014; Wilhelm et al., 2016). However, it is unclear whether knowledge gained from historical turbidites is also applicable to prehistoric turbidites which are vital for recovering a long earthquake archive. In addition, the synchronous deposition of turbidites cannot be verified if only one deep core is drilled in a depocenter. Here, we propose a new approach to authenticate the seismic origin and local seismic intensities for triggering prehistoric turbidites by analyzing the genetically linked *in situ* deformation of each turbidite preserved in a deep core from the Dead Sea center. The observed deformations in the lake center are similar to seismically induced deformations seen in lakes from other tectonically active regions such as California (Sims, 1973), Anatolia (Avşar et al., 2016), and Southern Italy (Moretti & Sabato, 2007; Vitale et al., 2019).

2. Sedimentary Regime and Previous Lacustrine Paleoseismology Research in the Dead Sea Basin

The sinistral strike-slip Dead Sea Fault forms the boundary between the Arabian and African plates, extending >1,000 km (Ben-Avraham et al., 2008). The ~150 km long and ~15 km wide Dead Sea Basin formed along this fault, and during the Quaternary this pull-apart basin received ~4 km of lacustrine sediments in its depocenter (Figure 1a) (Ben-Avraham et al., 2008). The sedimentary sequence comprises alternating laminae of aragonite and detritus (*aad;* Text S1) (Figure 1o), homogeneous mud (Figures 1n and 1o), gypsum (Figure 1b), halite (Figure 1c) (Neugebauer et al., 2014; Lu et al., 2017a, 2020a), and seismically disturbed units (Figures 1d–1m) (Lu et al., 2017b, 2020b). The first four types of sediment are regarded as background sedimentation (Text S2), while disturbed units including soft-sediment deformation, liquefied sand layers, slumps, chaotic deposits, and micro-faults have been interpreted as seismites (Heifetz et al., 2005; Ken-Tor et al., 2001; Lu et al., 2017b, 2020b; Marco & Agnon, 1995; Wetzler et al., 2010).

Widespread *in situ* soft-sediment deformation characterizes the Dead Sea sediments (Marco & Agnon, 1995; Lu et al., 2017b; Alsop et al., 2019), which manifests as several forms of (i) linear waves, (ii) asymmetric billows, (iii) coherent vortices, and (iv) intraclast breccias (Figures 1d–1m) (Lu et al., 2020b). The temporal correspondence of these structures with historic earthquakes (Ken-Tor et al., 2001; Migowski et al., 2004) and their juxtaposition against syn-depositional faults (Marco & Agnon, 1995) reveal that these deformations are seismites. In this study, we use *in situ* soft-sediment deformations and micro-faults to constrain the seismic origin and intensities of each overlying prehistoric turbidite. We also establish seven basic earthquake-related depositional scenarios for the lake depocenter.

3. Materials and Methods

The 457 m-long ICDP Core 5017-1 provides a record back to 220 ka (Goldstein et al., 2020) (Text S4). The surface of the archived half of the core was scanned with the ITRAX core scanner at a resolution of 1 mm, an exposure time of 1 s, and a Chromium tube at 30 kV voltage and 30 mA current at the GFZ (Potsdam) (Neugebauer et al., 2014). This X-ray fluorescence (XRF) core scanning highlights relative element intensities which can then be used to reveal sedimentary processes, although the absolute values could be influenced by down-core changes in physical properties such as grain size and water content (Neugebauer et al., 2016).

In Core 5017-1, gypsum has a high content of Ca and an extremely low Ti content (Figure 1b), while halite has extremely low concentrations of both Ca and Ti (Figure 1c). Detrital mud has a high content of Ti but low Ca content, while the aragonite laminae have a low content of Ti but high content of Ca (Figures 1n–1o). These features suggest that Ca best characterizes carbonate or gypsum, while Ti best reflects the input of exogenous clastics from the surrounding drainage basin. In addition, Ca and Ti both have sufficient count rates and were therefore chosen to characterize sediment layers, rather than transforming the elemental intensities into ratios or log-ratios (Weltje et al., 2015).

4. Results and Discussion

4.1. XRF Data Characterizes *In Situ* Seismites

Layers comprising linear waves, asymmetric billows, and coherent vortices (Figures 1d–1i) have similar variations of Ca and Ti to *aad* (Figure 1o). This indicates that no external sediments were incorporated during deformation as this would lead to significant variations in Ca and Ti. This relationship also confirms the *in situ* formation and preservation processes of these units. As micro-faults only displace sediments over short distances, they would not significantly alter the chemical features (Figures 1j and 1k).

The intraclast breccia layers consist of mixed *aad* fragments and relict pieces of coherent vortices in their lower parts. Large-scale intraclast breccia layers normally comprise three units: (i) unbroken coherent vortices at the base, (ii) remaining parts of coherent vortices and *aad* fragments in the middle, (iii) a gray-colored unit at the top (Figure 1l). The lower unit displays similar variations of Ca and Ti to *aad* and is sometimes absent in thinner intraclast breccia layers (Figure 1m). The middle unit shows a low content of Ca and high content of Ti due to the accumulation of large fragments of dark detritus laminae. Finally, the upper unit is marked by a high concentration of Ca and low concentration of Ti, indicating a local settling process during the final stages of brecciation. The delicate aragonite laminae were disaggregated into small particles and would therefore settle later than the larger fragments of coherent vortices and dark detritus laminae (the middle unit). The local mixing, sorting, and settling processes require open boundary conditions and a fluid environment at the sediment-water interface and cannot form beneath the sediment surface. These characters therefore validate the previous basic hypothesis that intraclast breccia layers formed at the sediment-water interface (Marco & Agnon, 1995). Chemical features of these units differ from homogeneous mud generated by floods (Figures 1n–1o), and thus confirm the *in situ* formation and preservation of intraclast breccia layers.

4.2. Establishing the Seismic Origin for Prehistoric Turbidites

We recorded >700 turbidites in the entire Core 5017-1 that are classified into three categories labeled 1–3: (1) sandy turbidites ($N = 9$) that temporally correlate with historic earthquakes (Lu et al., 2020b); (2) turbidites ($N = 136$) that overlie *in situ* seismites; (3) the remaining turbidites ($N > 560$) that lack underlying *in situ* seismites. The category 3 turbidites may be triggered either by earthquakes, or by non-seismic factors such as flooding, sediment overloading, and slope failures induced by changes in lake-levels. This study is focused on the category two turbidites and examines the possible links between turbidites and underlying *in situ* seismites. This allows us to then apply new insights into the category three turbidites, and thereby improve the completeness of the paleoseismic archive in the Dead Sea. We classify the category two turbidites into two basic types that are distinguished by distinct textures and geochemistry.

4.2.1. Type I: Sandy Turbidites

These turbidites are marked by a sandy base and usually show graded-bedding. Analysis from the base toward the top of individual turbidites reveals that some display only small variations in Ca and Ti (Figure 2f), some show a decrease of Ca and an increase of Ti (Figures 2g, 2k, and 2n), while others are marked by an increase of Ca but a decrease of Ti (Figures 2l and 2p). Other turbidites may display a decrease in both Ca and Ti at the base, and an increase of both Ca and Ti in the middle and upper parts (Figures 2c–2e and 2o). However, the Ti content of these turbidites is notably lower than homogeneous mud thereby making non-seismic causes such as flooding unlikely triggers for these turbidites (Figure 3b).

We find 33, 12, 15, 7, and 29 such turbidites immediately overlying layers containing linear waves, asymmetric billows, coherent vortices, intraclast breccia, and micro-fault, respectively, with no intervening background sediment preserved between the turbidite and deformed horizon (Figure 2; Figure S1). We infer that no depositional hiatus occurred directly beneath the turbidite as the drilling site is continuously below lake water levels. In detail, the drilling site was located in the abyssal plain of the lake depocenter with negligible slope gradients, and ~5 km from the nearest basin slopes (Lu et al., 2017b). This unique depositional environment does not favor strong erosion by turbidity flows above the *in situ* seismites (Figure S2). In such a tectonically active graben, this special combination of sediment layers makes seismic shaking the most plausible trigger for these turbidites. We therefore propose that these sandy turbidites are genetically linked to the underlying *in situ* seismites, and resulted from earthquake-triggered remobilization of nearshore surficial sediments.

The absence of background sediments between *in situ* deformation structures and overlying turbidites confirms the linkage between these features and highlights that deformation ocurred at the interface of water and sediments. These seismogenic turbidites appear to have no uniform chemical features, but show more variation in Ca and Ti than homogeneous mud (Figure 1n–1o), potentially indicating variability in the source material. In addition, some turbidite layers (Figures 2a–2c, 2k, and 2l) display amalgamated structure (Van Daele et al., 2017), that is, the superposition of different turbiditic flows typically triggered by an earthquake, which may also lead to non-uniform chemical features.

4.2.2. Type II: Laminae Fragments-Embedded Detritus Layers

Gray color and sparse *aad* fragments characterize these layers (Figure 4; Figure S3). The lack of relict fragments of coherent vortices in the lower part of the layers differentiates them from the intraclast breccia layers. The small size of fragments indicates that the *aad* have undergone significant transportation by high-density turbiditic flows instead of an *in situ* deformation process. Type II layers from the lake margin retain fragments of aragonite laminae (Figures 4a–4c; Migowski et al., 2004) that are much larger than those preserved in the lake center, which is consistent with significantly shorter transportation. The Type II layers from the lake center have high concentration of Ca and low concentration of Ti, with overall values similar to aragonite laminae (Figures 4d–4m and 3b) and the upper gray-colored units of intraclast breccia layers (Figures 1l and 1m). We interpret this to indicate a mixing process during mass transport. The upper parts of some Type II layers are commonly lighter in color and have a higher concentration of Ca, suggesting

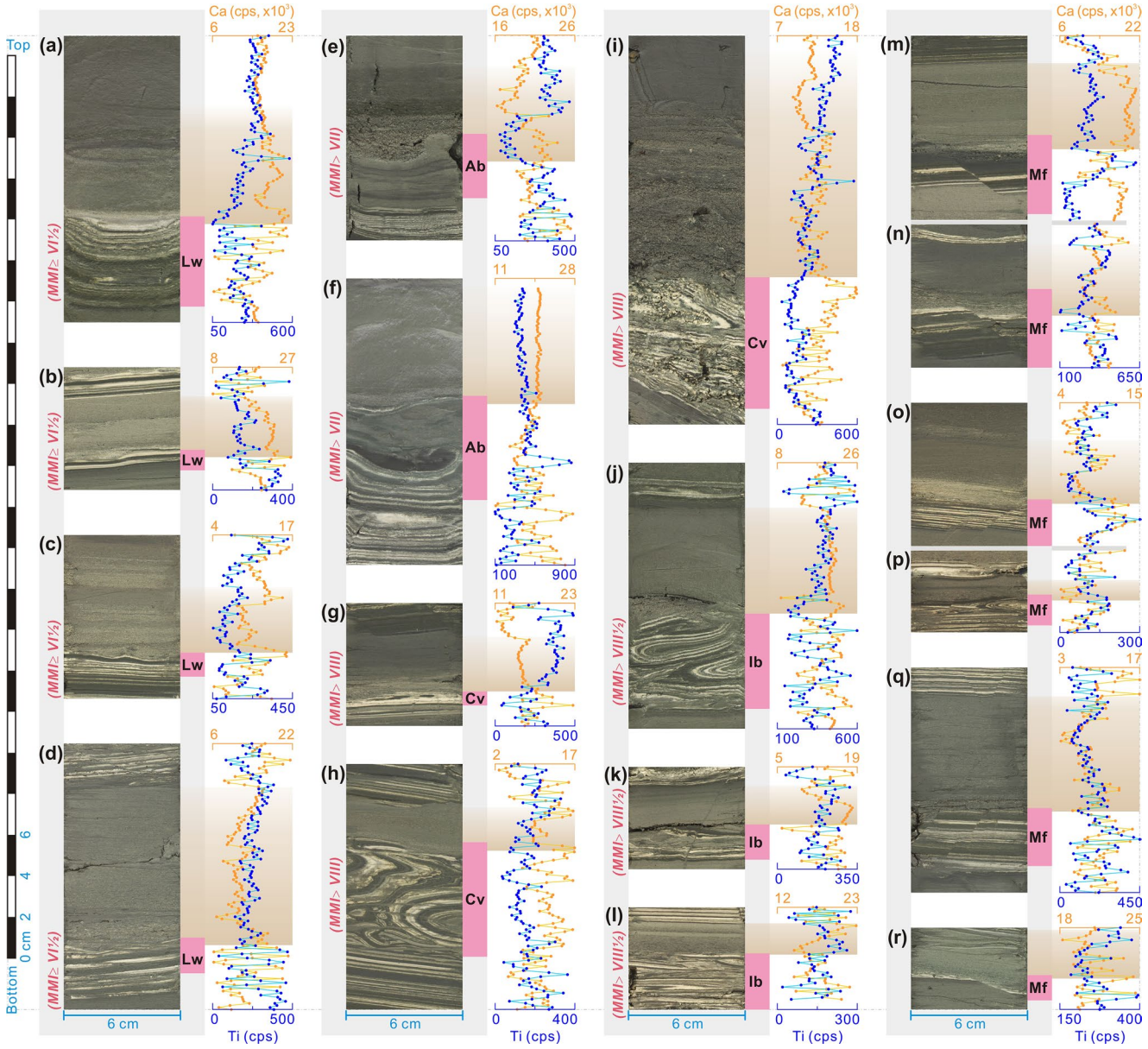

Figure 2. XRF data characterizing Type I turbidites from the Dead Sea center. (a–l) Turbidites (brown color) overlie *in situ* soft-sediment deformations (pink color). (m–r) Turbidites overlying micro-faults. See Text S5 for core depth.

that delicate aragonite laminae were broken into small particles not visible to the naked eye. In contrast, fragments of more robust (due to their cohesively and higher density) dark detrital laminae are much better preserved and comprise the lower parts of layers which display low Ca and high Ti (Figures 4f, 4j, and 4l).

Along the Dead Sea margin (Ein Gedi core; Figure 1a), such layers have been temporally correlated with historic earthquakes (Figures 4a–4c) (Agnon et al., 2006; Migowski et al., 2004). In Core 5017-1, we find 11, 2, 14, 3 and 10 such turbidites overlying layers of linear waves, asymmetric billows, coherent vortices, intraclast breccia, and micro-fault, respectively (Figures 4d–4m), implying a seismic origin of these sediments. We propose that Type II layers have resulted from seismogenic slope failure-induced breakage, fluidization, and suspension of *aad* fragments.

The lack of coarse clastic grains combined with the high concentrations of Ca and low concentrations of Ti suggest that Type II layers are most probably sourced from deeper subaqueous slopes rather than the

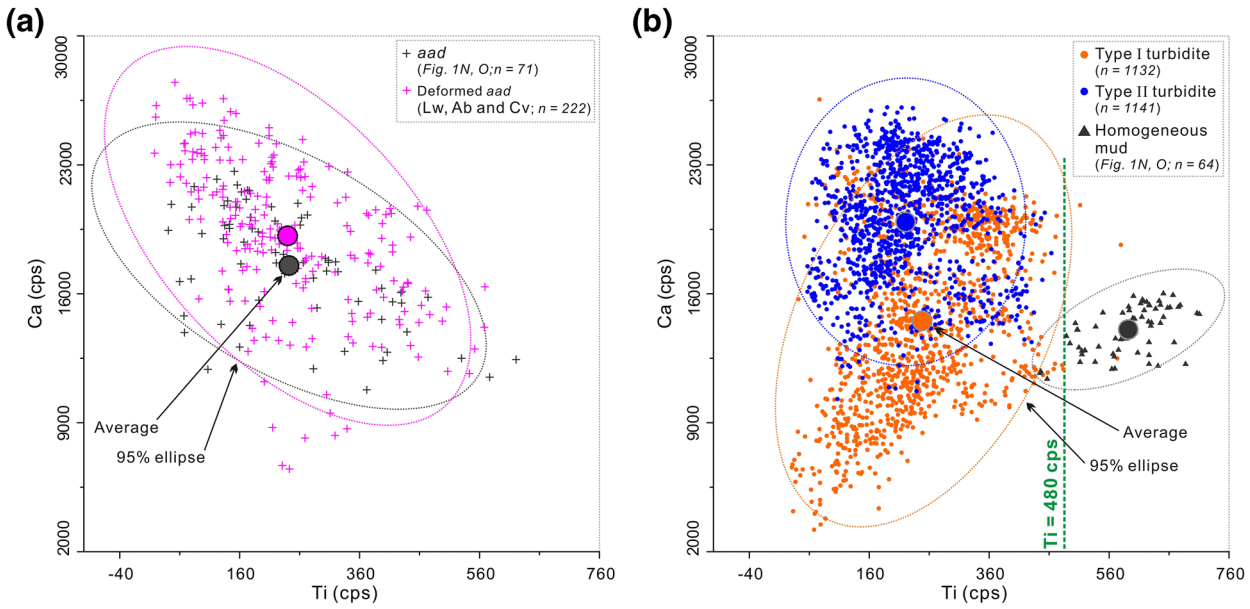

Figure 3. Scatter plots of Ca and Ti for different types of sediments. (a) Relatively similar clusters of *aad* and deformed *aad* (i.e., Lw, Ab, and Cv); (b) Type I turbidites, Type II turbidites, and homogeneous mud (generated by flash floods) from the Dead Sea center (Core 5017-1) group in distinct clusters. The *aad* and homogeneous mud are background deposits; n, number of data points. Lw, linear waves; Ab, asymmetric billows; Cv, coherent vortices.

nearshore region. These chemical and physical features differentiate Type II layers from any hyperpycnal flow deposits generated by flash floods, which lack laminae fragments and have low concentrations of Ca but high concentrations of Ti (Figures 1n–1o and 3b). Therefore, we infer that the remaining turbidites with similar textures and chemical features to the Type II layers, but lacking underlying *in situ* seismites (~178 of the category 3 turbidites), were also the product of seismogenic subaqueous slope failures (Figures 4l–4p).

4.3. Constraining the Seismic Intensities that Triggered Individual Prehistoric Turbidites

A series of fluid dynamic numerical models, based on the Kelvin-Helmholtz Instability, have been conducted to simulate the soft-sediment deformation processes (Heifetz et al., 2005; Lu et al., 2020b; Wetzler et al., 2010). This modeling indicates minimum ground accelerations of 0.13 g, 0.18 g, 0.34 g, and 0.50 g are needed to initiate linear waves, asymmetric billows, coherent vortices, and intraclast breccia with a certain thickness, respectively (Lu et al., 2020b). These accelerations are converted into Modified Mercalli Intensity (MMI) Scale of VI½, VII, VIII, and VIII½, respectively, via empirical relationships between MMI and peak ground acceleration for a transform boundary setting (Lu et al., 2020b; Wald et al., 1999).

The *in situ* soft-sediment deformations that underly 67 Type I and 30 Type II layers constrain the local seismic intensities that triggered these prehistoric turbidites as varying from MMI of ~≥VI½ to >VIII½ (Figures 2 and 4; Lu et al., 2020b). Thus, the dataset suggests an intensity threshold of MMI VI½ for triggering centimeter-scale prehistoric turbidites preserved in the Dead Sea center. Previous studies have revealed that the intensity threshold for triggering historic turbidites are variable in different regions and range from MMI V½ to VII½ (Howarth et al., 2014; Moernaut, 2020; Van Daele et al., 2015; Wilhelm et al., 2016). The intensity threshold constrained from the Dead Sea data (~≥VI½) is situated in the middle of this range.

Previous studies in Chilean lakes have indicated that the (cumulative) thickness of historic turbidites across multiple cores correlates with seismic intensity, and can thus be used to infer paleo-intensities in this setting (Moernaut et al., 2014). However, in the case of the Dead Sea core 5017-1, there is a random relationship (a correlation factor of 0.04) between the thickness of prehistoric turbidites and seismic intensity (Figure 5a). Each type of *in situ* deformation (representing different MMI levels) is overlain by turbidites of variable thicknesses (Figures 2 and 4). This discrepancy may be due to different conditions regarding available slope materials affected by seismic shaking in the two different tectonic settings. Moreover, the absence of an

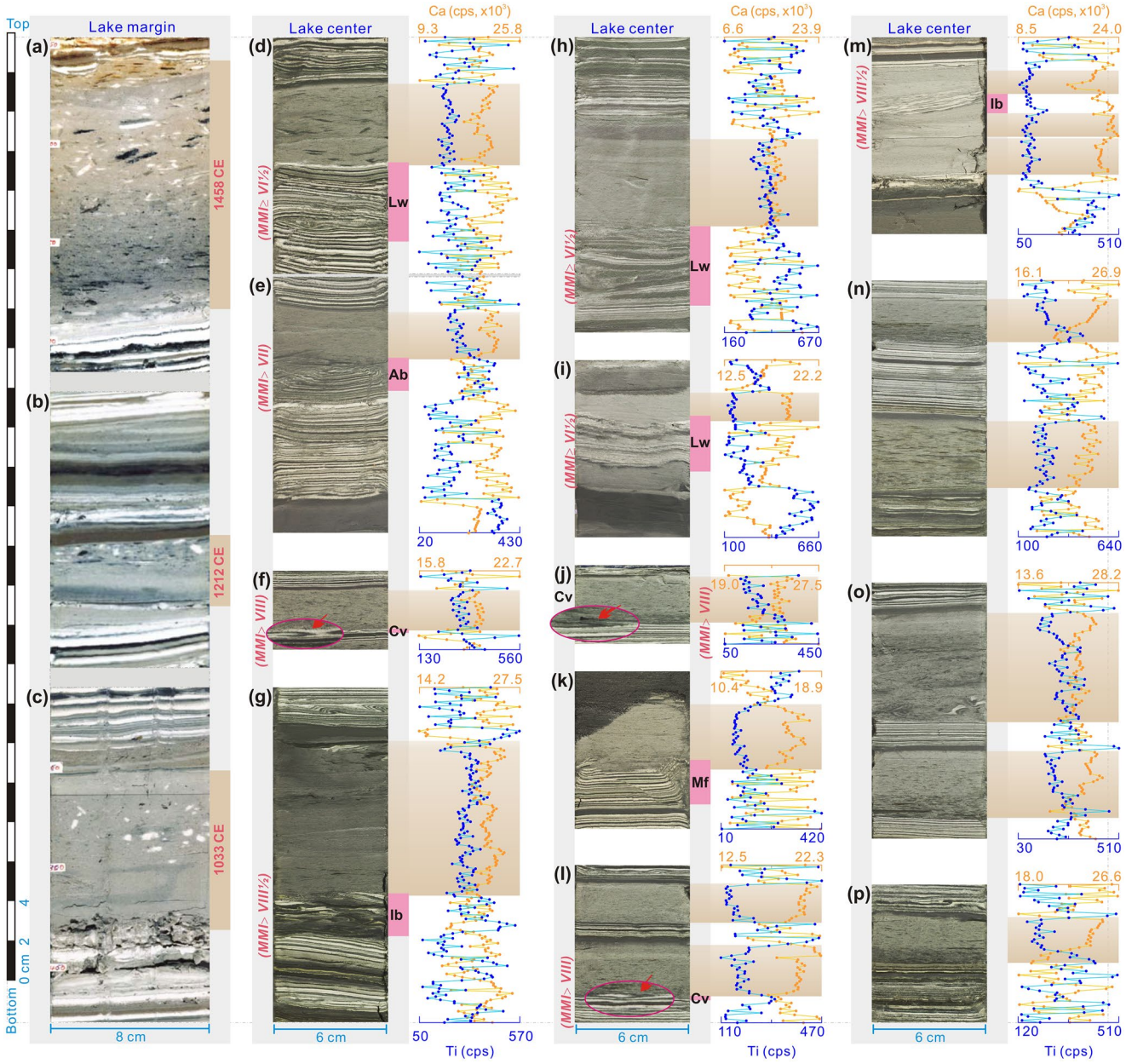

Figure 4. XRF data characterizing Type II turbidites (the laminae fragments-embedded detritus layers) from the lake center (Core 5017-1). (a–c) The layers from the lake margin (Ein Gedi core) that correlate with historic earthquakes (Agnon et al., 2006; Migowski et al., 2004) are used for comparison. (d–k) The layers from the lake center (brown color) are overlying *in situ* seismites. (l–p) The layers from the lake center without underlying *in situ* seismites. The red arrows indicate the remaining parts of Cv; the magenta circles are magnifying glasses (2.5X). See Text S6 for core depth.

intensity-thickness relationship in the Dead Sea may be caused by high-amplitude lake level fluctuations that strongly influence the type and rate of slope sediment deposition, and by subtle micro-topography produced by each *in situ* deformation which modulates turbidite deposition. Therefore, caution is needed when applying turbidite thicknesses to reconstruct paleo-intensities in different geological settings.

4.4. Models of Earthquake-Related Deposition and Paleoseismic Implications

Based on studies from the Dead Sea, we propose seven basic earthquake-related depositional scenarios in a lake depocenter (Figures 5b and 5c). Each scenario represents a single seismic event. Scenario I, an *in situ*

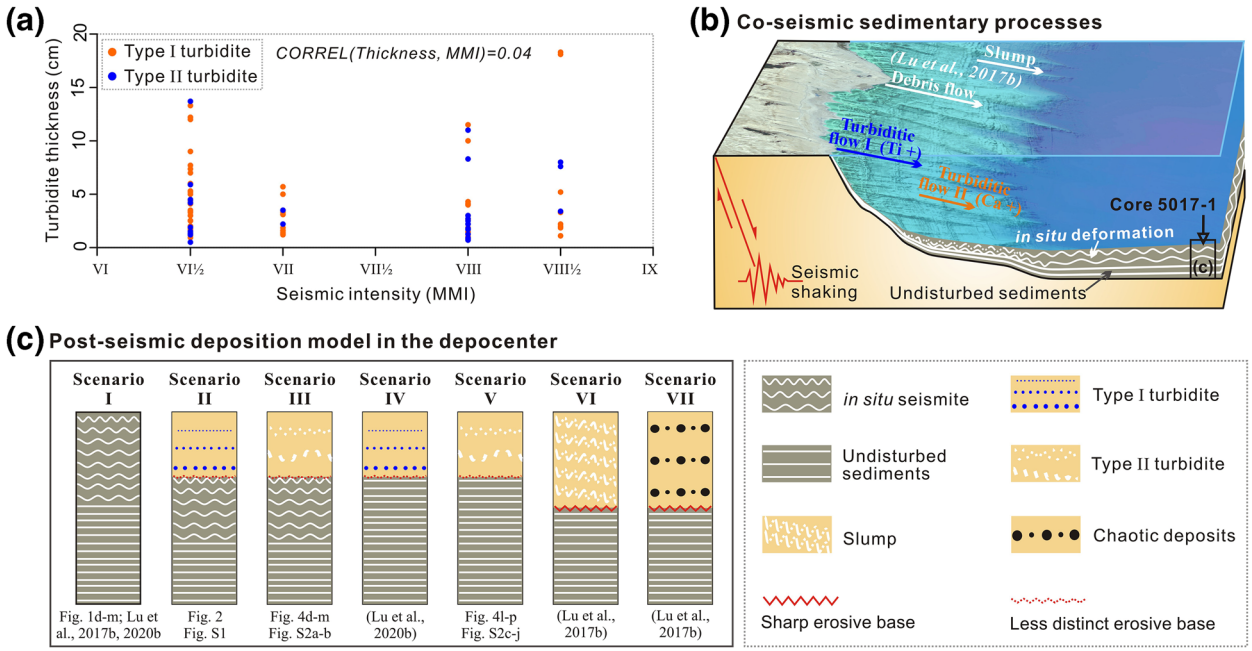

Figure 5. Seismogenic sedimentary processes and deposition models in the Dead Sea. (a) Random relationship between the thickness of prehistoric turbidites and seismic intensity. (b) Schematic model showing co-seismic sedimentary processes in the lake. (c) Earthquake-related deposition models in the lake depocenter. See the text for a detailed interpretation.

seismite overlying undisturbed sediments. This situation is recorded from the lake margin and has been used to reconstruct the earthquake history of the Dead Sea Fault over the last 70 kyr (Ken-Tor et al., 2001; Marco et al., 1996; Migowski et al., 2004). Moreover, based on numerical simulation of the *in situ* deformation processes and its application to Core 5017-1, Lu et al. (2020b) revealed and quantified the history of large earthquakes along the central Dead Sea Fault over the past 220 kyr.

Scenario II involves sandy turbidite overlying an *in situ* seismite, while scenario III encompasses Type II turbidite overlying an *in situ* seismite. These two situations are helpful for a better understanding of seismogenic turbiditic flows by constraining the intensity threshold for triggering turbidites. In Scenario IV, the sandy turbidite lacks an underlying *in situ* seismite but is temporally correlated with a historic earthquake (Lu et al., 2020b). Scenario V involves a Type II turbidite that lacks an underlying *in situ* seismite. This scenario is observed in the Dead Sea margin and has been temporally correlated to historic earthquakes (Agnon et al., 2006; Migowski et al., 2004). Scenarios VI and VII are slump and chaotic deposits without underlying *in situ* seismites, respectively (Lu et al., 2017b).

Among the models, *in situ* seismites are missing in scenarios IV, V, VI, and VII. We find sharp erosive bases for scenarios VI and VII, and less distinct erosive bases for some of scenarios II-V (Figure S2). We infer that in scenarios VI and VII, any *in situ* seismites, which would be positioned below the seismogenic deposits, have been eroded by the earthquake-induced energetic mass movements. While, in scenarios IV and V, the lack of *in situ* seismites is either due to their formation not being favored by the lithology or due to poor preservation of the deformation structures. The seismogenic sediment layers in scenarios IV, V, VI, and VII could be used as independent earthquake indicators, and are thus vital for complete paleoseismic reconstructions in the region and similar tectonic settings elsewhere.

5. Conclusions

We constrain seismic origin of two types of turbidites by analyzing their underlying *in situ* seismites, then apply the new insights into some turbidites that lack underlying *in situ* seismites, and thereby improve the completeness of the paleoseismic archive in the Dead Sea. In addition, we propose seven basic post-seismic depositional scenarios in a lake depocenter that is located in a tectonically active region like the Dead

Sea. These techniques and findings are vital for more complete paleoseismic reconstructions, and greater confidence in assessing geohazards in tectonically active regions like the Dead Sea. Moreover, our high-resolution chemical and sedimentological data validate a previous hypothesis that soft-sediment deformation in the Dead Sea formed at the sediment-water interface.

Data Availability Statement

Data are available in the PANGAEA database (https://doi.pangaea.de/10.1594/PANGAEA.921987).

Acknowledgments
The authors appreciate the editor Lucy Flesch for handling our manuscript, Stefano Vitale and Alina Polonia for constructive reviews. This research was supported by the University of Liege under Special Funds for Research, IPD-STEMA Program (R.DIVE.0899-J-F-G to Y. Lu), Austrian Science Fund (FWF: M 2817 to Y. Lu), the DESERVE Virtual Institute of the Helmholtz Association (to A. Agnon), the Israel Science Foundation (#1093/10 to R.Bookman and #1645/19 to S.Marco), and the ICDP.

References

Agnon, A., Migowski, C., & Marco, S. (2006). Intraclast breccias in laminated sequences reviewed: Recorders of paleo-earthquakes. *Geological Society of America Special Paper*, *401*, 195–214. https://doi.org/10.1130/2006.2401(13)

Alsop, G. I., Weinberger, R., Marco, S., & Levi, T. (2019). Identifying soft-sediment deformation in rocks. *Journal of Structural Geology*, *125*, 248–255. https://doi.org/10.1016/j.jsg.2017.09.001

Avşar, U., Jónsson, S., Avşar, Ö., & Schmidt, S. (2016). Earthquake-induced soft-sediment deformations and seismically amplified erosion rates recorded in varved sediments of Köyceğiz Lake (SW Turkey). *Journal of Geophysical Research: Solid Earth*, *121*(6), 4767–4779. https://doi.org/10.1002/2016JB012820

Bartov, Y., Agnon, A., Enzel, Y., & Stein, M. (2006). Late Quaternary faulting and subsidence in the central Dead Sea basin. *Israel Journal of Earth Sciences*, *55*, 17–31.

Ben-Avraham, Z., Garfunkel, Z., & Lazar, M. (2008). Geology and evolution of the southern Dead Sea Fault with emphasis on subsurface structure. *Annual Review of Earth and Planetary Sciences*, *36*, 357–387.

Clare, M. A., Hughes Clarke, J. E., Talling, P. J., Cartigny, M. J. B., & Pratomo, D. G. (2016). Preconditioning and triggering of offshore slope failures and turbidity currents revealed by most detailed monitoring yet at a fjord-head delta. *Earth and Planetary Science Letters*, *450*, 208–220. https://doi.org/10.1016/j.epsl.2016.06.021

Goldfinger, C., Morey, A. E., Nelson, C. H., Gutiérrez-Pastor, J., Johnson, J. E., Karabanov, E., et al. (2007). Rupture lengths and temporal history of significant earthquakes on the offshore and north coast segments of the Northern San Andreas Fault based on turbidite stratigraphy. *Earth and Planetary Science Letters*, *254*(1–2), 9–27. https://doi.org/10.1016/j.epsl.2006.11.017

Goldfinger, C., Nelson, C. H., & Johnson, J. E. (2003). Holocene earthquake records from the cascadia subduction zone and northern San Andreas fault based on precise dating of offshore turbidites. *Annual Review of Earth and Planetary Sciences*, *31*(1), 555–577. https://doi.org/10.1146/annurev.earth.31.100901.141246

Goldstein, S. L., Kiro, Y., Torfstein, A., Kitagawa, H., Tierney, J., & Stein, M. (2020). Revised chronology of the ICDP Dead Sea deep drill core relates drier-wetter-drier climate cycles to insolation over the past 220 kyr. *Quaternary Science Reviews*, *244*, 106460. https://doi.org/10.1016/j.quascirev.2020.106460

Gràcia, E., Vizcaino, A., Escutia, C., Asioli, A., Rodés, Á., Pallàs, R., et al. (2010). Holocene earthquake record offshore Portugal (SW Iberia): Testing turbidite paleoseismology in a slow-convergence margin. *Quaternary Science Reviews*, *29*(9–10), 1156–1172. https://doi.org/10.1016/j.quascirev.2010.01.010

Heifetz, E., Agnon, A., & Marco, S. (2005). Soft sediment deformation by Kelvin Helmholtz Instability: A case from Dead Sea earthquakes. *Earth and Planetary Science Letters*, *236*(1–2), 497–504. https://doi.org/10.1016/j.epsl.2005.04.019

Howarth, J. D., Fitzsimons, S. J., Norris, R. J., & Jacobsen, G. E. (2014). Lake sediments record high intensity shaking that provides insight into the location and rupture length of large earthquakes on the Alpine Fault, New Zealand. *Earth and Planetary Science Letters*, *403*, 340–351. https://doi.org/10.1016/j.epsl.2014.07.008

Hubert-Ferrari, A., Lamair, L., Hage, S., Schmidt, S., Çağatay, M. N., & Avşar, U. (2020). A 3800 yr paleoseismic record (Lake Hazar sediments, eastern Turkey): Implications for the East Anatolian Fault seismic cycle. *Earth and Planetary Science Letters*, *538*, 116152.

Katz, T., Ginat, H., Eyal, G., Steiner, Z., Braun, Y., Shalev, S., and Goodman-Tchernov, B. N. (2015). Desert flash floods form hyperpycnal flows in the coral-rich Gulf of Aqaba, Red Sea. *Earth and Planetary Science Letters*, *417*, 87–98. https://doi.org/10.1016/j.epsl.2015.02.025

Ken-Tor, R., Agnon, A., Enzel, Y., Stein, M., Marco, S., & Negendank, J. F. W. (2001). High-resolution geological record of historic earthquakes in the Dead Sea basin. *Journal of Geophysical Research*, *106* (B2), 2221–2234.

Kioka, A., Schwestermann, T., Moernaut, J., Ikehara, K., Kanamatsu, T., Eglinton, T., & Strasser, M. (2019). Event stratigraphy in a hadal oceanic trench: The Japan Trench as sedimentary archive recording recurrent giant subduction zone earthquakes and their role in organic carbon export to the deep sea. *Frontiers in Earth Science*, *7*.

Lu, Y., Bookman, R., Waldmann, N., & Marco, S. (2020a). A 45 kyr laminae record from the Dead Sea: Implications for basin erosion and floods recurrence. *Quaternary Science Reviews*, *229*, 106143. https://doi.org/10.1016/j.quascirev.2019.106143

Lu, Y., Waldmann, N., Ian Alsop, G., & Marco, S. (2017b). Interpreting soft sediment deformation and mass transport deposits as seismites in the Dead Sea depocenter. *Journal of Geophysical Research: Solid Earth*, *122*, 8305–8325.

Lu, Y., Waldmann, N., Nadel, D., & Marco, S. (2017a). Increased sedimentation following the neolithic revolution in the southern Levant. *Global and Planetary Change*, *152*, 199–208. https://doi.org/10.1016/j.gloplacha.2017.04.003

Lu, Y., Wetzler, N., Waldmann, N., Agnon, A., Biasi, G., & Marco, S. (2020b). A 220,000 years-long continuous large earthquake record on a slow-slipping plate boundary. *Science Advances*, *6*, eaba4170. https://doi.org/10.1126/sciadv.aba4170

Marco, S., & Agnon, A. (1995). Prehistoric earthquake deformations near Masada, Dead Sea graben. *Geology*, *23*(8), 695–698.

Marco, S., Stein, M., Agnon, A., & Ron, H. (1996). Long-term earthquake clustering: A 50,000 years paleoseismic record in the Dead Sea Graben. *Journal of Geophysical Research*, *101*, 6179–6192.

Migowski, C., Agnon, A., Bookman, R., Negendank, J. F. W., & Stein, M. (2004). Recurrence pattern of Holocene earthquakes along the Dead Sea transform revealed by varve-counting and radiocarbon dating of lacustrine sediments. *Earth and Planetary Science Letters*, *222*(1), 301–314. https://doi.org/10.1016/j.epsl.2004.02.015

Moernaut, J. (2020). Time-dependent recurrence of strong earthquake shaking near plate boundaries: A lake sediment perspective. *Earth-Science Reviews*, *210*, 103344. https://doi.org/10.1016/j.earscirev.2020.103344

Moernaut, J., Daele, M. V., Heirman, K., Fontijn, K., Strasser, M., Pino, M., et al. (2014). Lacustrine turbidites as a tool for quantitative earthquake reconstruction: New evidence for a variable rupture mode in south central Chile. *Journal of Geophysical Research: Solid Earth*, *119*(3), 1607–1633. https://doi.org/10.1002/2013jb010738

Moernaut, J., Van Daele, M., Fontijn, K., Heirman, K., Kempf, P., Pino, M., et al. (2018). Larger earthquakes recur more periodically: New insights in the megathrust earthquake cycle from lacustrine turbidite records in south-central Chile. *Earth and Planetary Science Letters*, *481*, 9–19. https://doi.org/10.1016/j.epsl.2017.10.016

Moretti, M., & Sabato, L. (2007). Recognition of trigger mechanisms for soft-sediment deformation in the Pleistocene lacustrine deposits of the Sant'Arcangelo Basin (Southern Italy): Seismic shock vs. overloading. *Sedimentary Geology*, *196*(1-4), 31–45. https://doi.org/10.1016/j.sedgeo.2006.05.012

Neugebauer, I., Brauer, A., Schwab, M. J., Waldmann, N. D., Enzel, Y., Kitagawa, H., et al. (2014). Lithology of the long sediment record recovered by the ICDP Dead Sea Deep Drilling Project (DSDDP). *Quaternary Science Reviews*, *102*, 149–165. http://dx.doi.org/10.1016/j.quascirev.2014.08.013

Neugebauer, I., Schwab, M. J., Waldmann, N. D., Tjallingii, R., Frank, U., Hadzhiivanova, E., et al. (2016). Hydroclimatic variability in the Levant during the early last glacial (~117-75 ka) derived from micro-facies analyses of deep Dead Sea sediments. *Climate of the Past*, *12*(1), 75–90. https://doi.org/10.5194/cp-12-75-2016

Paull, C. K., Talling, P. J., Maier, K. L., Parsons, D., Xu, J., Caress, D. W., et al. (2018). Powerful turbidity currents driven by dense basal layers. *Nature Communications*, *9*(1), 4114. https://doi.org/10.1038/s41467-018-06254-6

Polonia, A., Panieri, G., Gasperini, L., Gasparotto, G., Bellucci, L. G., & Torelli, L. (2013). Turbidite paleoseismology in the Calabrian arc subduction complex (Ionian sea). *Geochemistry, Geophysics, Geosystems*, *14*(1), 112–140. https://doi.org/10.1029/2012gc004402

Polonia, A., Vaiani, S. C., & de Lange, G. J. (2016). Did the A.D. 365 Crete earthquake/tsunami trigger synchronous giant turbidity currents in the Mediterranean Sea? *Geology*, *44*(3), 191–194. https://doi.org/10.1130/g37486.1

Pouderoux, H., Proust, J.-N., & Lamarche, G. (2014). Submarine paleoseismology of the northern Hikurangi subduction margin of New Zealand as deduced from Turbidite record since 16 ka. *Quaternary Science Reviews*, *84*, 116–131. https://doi.org/10.1016/j.quascirev.2013.11.015

Ratzov, G., Cattaneo, A., Babonneau, N., Deverchere, J., Yelles, K., Bracene, R., and Courboulex, F. (2015). Holocene turbidites record earthquake supercycles at a slow-rate plate boundary. *Geology*, *43*(4), 331–334. https://doi.org/10.1130/g36170.1

Sims, J. D. (1973). Earthquake-induced structures in sediments of Van Norman Lake, San Fernando, California. *Science*, *182*(4108), 161–163.

St-Onge, G., Mulder, T., Piper, D. J. W., Hillaire-Marcel, C., & Stoner, J. S. (2004). Earthquake and flood-induced turbidites in the Saguenay Fjord (Québec): A holocene paleoseismicity record. *Quaternary Science Reviews*, *23*(3–4), 283–294. https://doi.org/10.1016/j.quascirev.2003.03.001

Strasser, M., Monecke, K., Schnellmann, M., Anselmetti, F. S., & Weissurt, H. (2013). Lake sediments as natural seismographs: A compiled record of Late Quaternary earthquakes in Central Switzerland and its implication for Alpine deformation. *Sedimentology*, *60*(1), 319–341. https://doi.org/10.1111/sed.12003

Talling, P. J., Paull, C. K., & Piper, D. J. W. (2013). How are subaqueous sediment density flows triggered, what is their internal structure and how does it evolve? Direct observations from monitoring of active flows. *Earth-Science Reviews*, *125*, 244–287. https://doi.org/10.1016/j.earscirev.2013.07.005

Van Daele, M., Meyer, I., Moernaut, J., De Decker, S., Verschuren, D., & De Batist, M. (2017). A revised classification and terminology for stacked and amalgamated turbidites in environments dominated by (hemi) pelagic sedimentation. *Sedimentary Geology,* (357), 72–82.

Van Daele, M., Moernaut, J., Doom, L., Boes, E., Fontijn, K., Heirman, K., et al. (2015). A comparison of the sedimentary records of the 1960 and 2010 great Chilean earthquakes in 17 lakes: Implications for quantitative lacustrine palaeoseismology. *Sedimentology*, *62*(5), 1466–1496. https://doi.org/10.1111/sed.12193

Vitale, S., Isaia, R., Ciarcia, S., Di Giuseppe, M. G., Iannuzzi, E., Prinzi, E. P., et al. (2019). Seismically induced soft-sediment deformation phenomena during the volcano-tectonic activity of Campi Flegrei caldera (southern Italy) in the last 15 kyr. *Tectonics*, *38*(6), 1999–2018.

Wald, D. J., Quitoriano, V., Heaton, T. H., & Kanamori, H. (1999). Relationships between peak ground acceleration, peak ground velocity, and modified Mercalli intensity in California. *Earthquake Spectra*, *15*(3), 557–564.

Weltje, G. J., Bloemsma, M., Tjallingii, R., Heslop, D., Röhl, U., & Croudace, I. W. (2015). Prediction of geochemical composition from XRF core scanner data: A new multivariate approach including automatic selection of calibration samples and quantification of uncertainties, In *Micro-XRF studies of sediment cores*, edited (pp. 507–534), Springer.

Wetzler, N., Marco, S., & Heifetz, E. (2010). Quantitative analysis of seismogenic shear-induced turbulence in lake sediments. *Geology*, *38*(4), 303–306. https://doi.org/10.1130/g30685.1

Wilhelm, B., Nomade, J., Crouzet, C., Litty, C., Sabatier, P., Belle, S., et al. (2016). Quantified sensitivity of small lake sediments to record historic earthquakes: Implications for paleoseismology. *Journal of Geophysical Research: Earth Surface*, *121*(1), 2–16. https://doi.org/10.1002/2015jf003644